SUPPORTING INFORMATION

Chinese Journal of Structural Chemistry

Phytate-Coordination Triggered Enrichment of Surface NiOOH Species on Nickel Foam for Efficient Urea Electrooxidation

Jiayuan Li[1#*], Yuefei Li[1#], Qingyu Xue[1], Yuchi Gao[1] and Yuanyuan Ma[1]

[1]*Key Laboratory of Special Functional and Smart Polymer Materials of Ministry of Industry and Information Technology, School of Chemistry and Chemical Engineering, Northwestern Polytechnical University, Xi'an 710072, China*

**Corresponding author. Email: Jiayuanli@nwpu.edu.cn*

[#] These authors contributed equally to this work.

n EXPERIMENTAL SECTION

Synthesis of phytate-coordinated nickel foam (PA-NF). Firstly, a piece of commercially available NF (1 cm × 1 cm) was firstly immerse in 1.0 M HCl solution for 15 min and washed with acetone and ethanol to remove surface impurities and oxides. A piece of NF was dipped in the 70 mL aqueous solution containing 3.0 mL phytic acid for 10 min. Then, the solution was transferred into a 100 mL Teflon-lined stainless-steel autoclave and maintained at 120 °C for 6 h. The as-synthesized electrode was rinsed with water several times and dried at 60 °C in vacuum for 8 h ready for use. As blank control, the NF was treated under the identical conditions in the absence of phytic acid. If not otherwise specified, the NF mentioned in the manuscript represents this treated electrode.

Characterization. X-ray diffraction (XRD) measurements were conducted on Ultima IV with Cu Kα radiation (λ = 0.1541 nm) from 10° to 90° at 40 kV and 40 mA. The morphology and energy dispersive X-ray (EDX) mapping of samples were analyzed by a ZEISS MERLIN Compact and Oxford X-max operated at an acceleration voltage of 30.0 kV. Fourier-transform infrared (FT-IR, Thermo Scientific Nicolet iS5) spectroscopy was used to measure the functional group of PA on the NF surface. X-ray photoelectron spectra (XPS) were measured using a Thermo Scientific K-Alpha equipped with Al Kα monochromatized radiation at 1486.6 eV X-ray source. All binding energies were referenced to the C 1s peak (284.6 eV) arising from the adventitious carbon-containing species. Raman spectra were acquired on an INVIAREFLEX Raman Spectrophotometer with an exciting wavelength of 532 nm.

Electrochemical Measurements. Electrochemical experiments were conducted on a CHI-760E Electrochemical Workstation (CHI Instruments) typically consisting of a standard three-electrode system. The electrochemical investigations of urea oxidation reaction (UOR) were performed at room temperature using a saturated calomel electrode (SCE) as reference electrode, a graphite rod as counter electrode, and a piece of PA-NF or bare NF served as a working electrode, respectively. 1.0 M KOH solution (40 mL) with or without urea was employed. The measured potentials versus the reversible hydrogen electrode (RHE) were calculated according to Equation (1):

$$E(\mathrm{RHE}) = E(\mathrm{SCE}) + 0.242\ \mathrm{V} + 0.0591 \times \mathrm{pH} = E(\mathrm{SCE}) + 1.068\ \mathrm{V} \quad (1)$$

All electrochemical investigations were carried out at room temperature (25 ± 1 °C), and the electrolyte was stirred at 800 rpm with a magnetic stir bar. Cyclic voltammetry (CV) measurements were performed at a scan rate of 5 mV/s. *Operando* electrochemical impedance spectroscopy (EIS) tests were performed at different applied potentials versus RHE in the frequency range of 0.01-100 k Hz was performed by using Autolab PGSTAT302N.

n SUPPLEMENTARY FIGURES AND TABLES

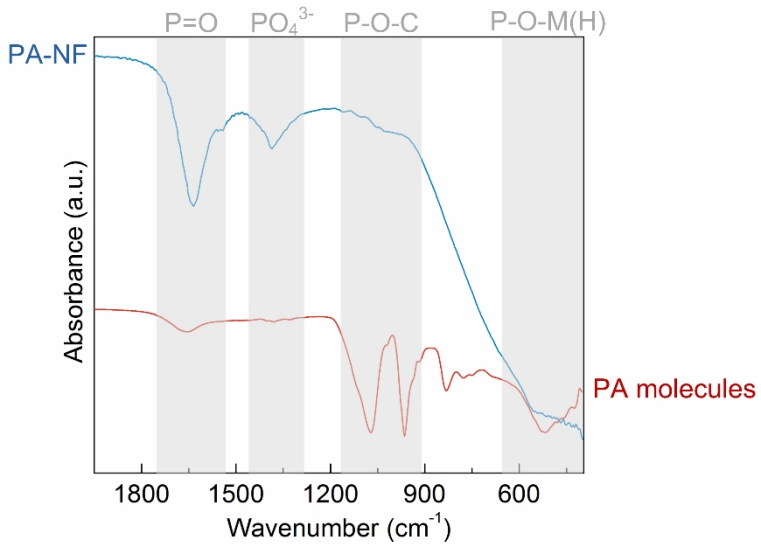

Figure S1. FT-IR spectra of the PA-NF and PA molecules.

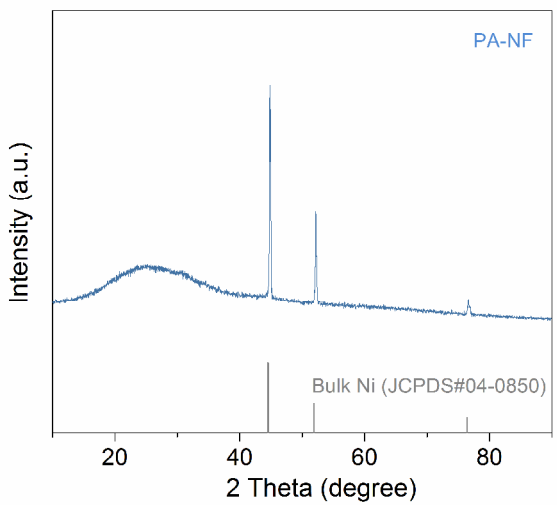

Figure S2. XRD spectrum of PA-NF.

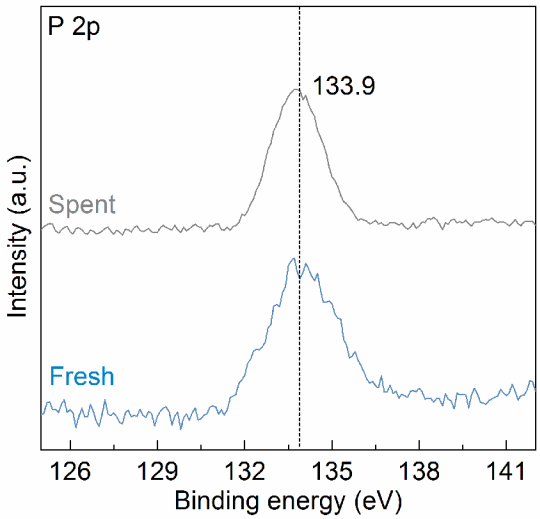

Figure S3. High-resolution XPS spectra of fresh and spent PA-NF in P 2p region.

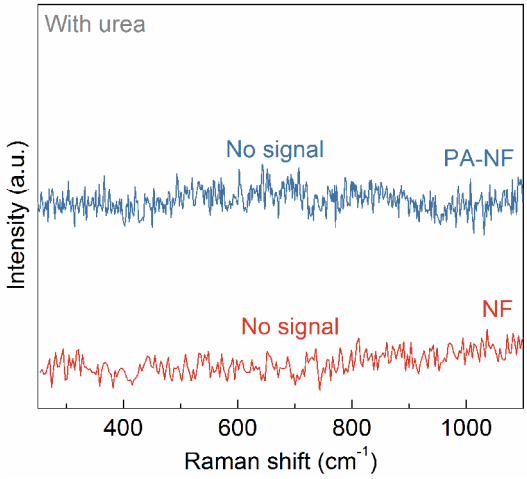

Figure S4. Raman spectra of the spent PA-NF and NF after UOR when the electrolyte contained urea.

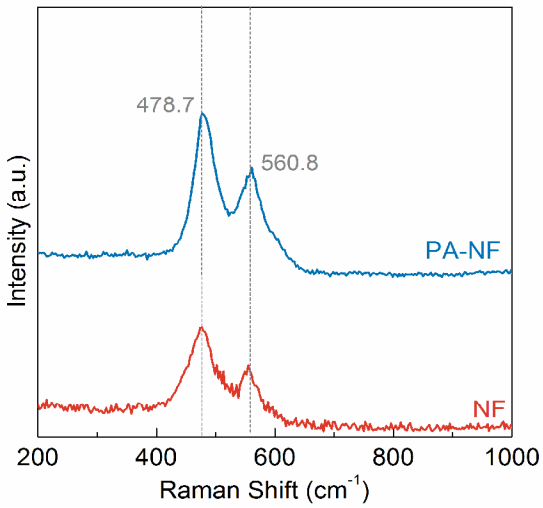

Figure S5. Raman spectra of the spent PA-NF and NF after UOR when the electrolyte does not contain urea.

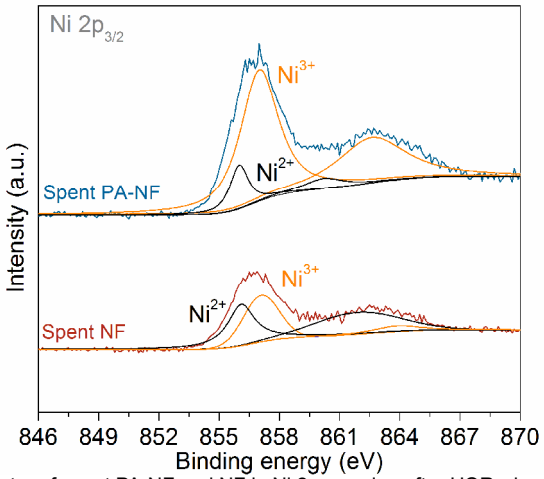

Figure S6. High-resolution XPS spectra of spent PA-NF and NF in Ni $2p_{3/2}$ region after UOR when the electrolyte did not contain urea.

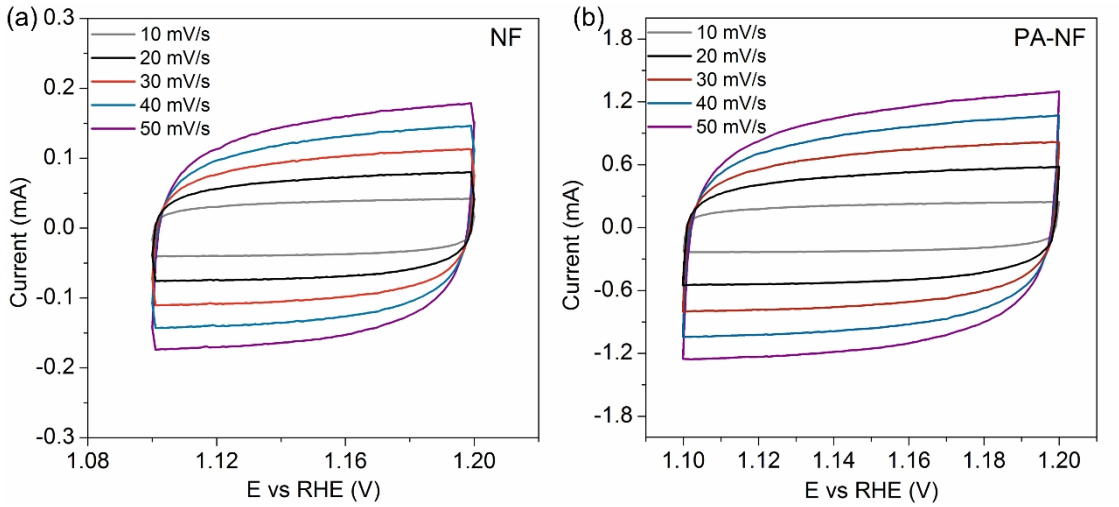

Figure S7. CV curves of (a) NF and (b) PA-NF electrodes with various scan rates in 1.0 M KOH with urea.

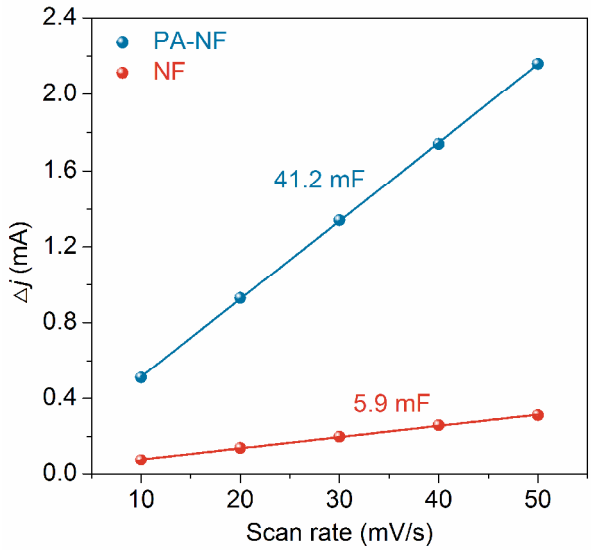

Figure S8. C_{dl} calculated from the CV curves in Figure S7.

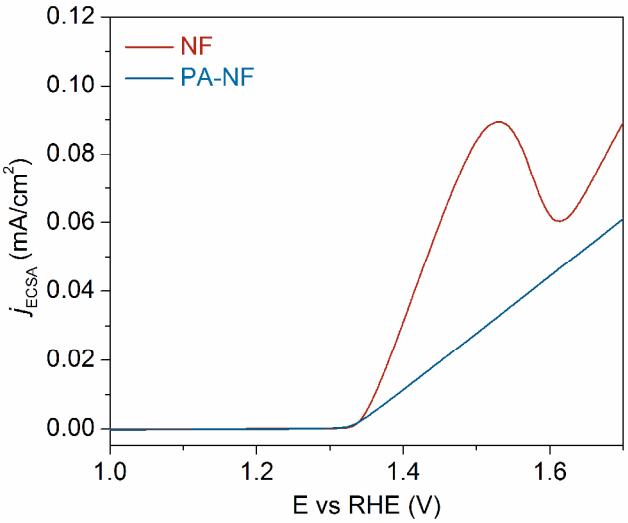

Figure S9. UOR activity for the PA-NF and NF electrodes normalized to ECSA.

Table S1. Comparison of Catalytic Performance of the PA-NF with the State-of-the-art Electrocatalysts for UOR in Alkaline Media

Catalyst	Electrolyte	E_{10} [V vs. RHE]	Tafel slope [mV/dec]	Ref.
PA-NF	1.0 M KOH + 0.33 M urea	1.38	64.1	This work
NF	1.0 M KOH + 0.33 M urea	1.65	168.2	This work
N-NiS	1.0 M KOH + 0.33M urea	1.62	158.0	Ref. [1]
N-NiS_2	1.0 M KOH + 0.33 M urea	1.62	186.0	Ref. [1]
$Ni(OH)_2$ NA/CC	1.0 M KOH + 0.33 M urea	1.81	180.0	Ref. [2]
Ni_3N NA/CC	1.0 M KOH + 0.33 M urea	1.44	172.0	Ref. [2]
RuO_2	1.0 M KOH + 0.33 M urea	1.53	125.0	Ref. [2]
2D NiS_2/Ti	1.0 M KOH + 0.5 M urea	1.82	144.6	Ref. [3]
$NiTe_2/Ni(OH)_2$	1.0 M KOH + 0.33 M urea	1.42	133.0	Ref. [4]
$Co_3O_4@Co_2P_4O_{12}$	1.0 M KOH + 0.5 M urea	1.56	126.0	Ref. [5]
$MnO_2/MnCo_2O_4/Ni$	1.0 M KOH + 0.5 M urea	1.58	72.0	Ref. [6]
Ni/C-1	1.0 M KOH + 0.3 M urea	1.60	77.0	Ref. [7]
Ni_2P/CFC	1.0 M KOH + 0.33 M urea	1.40	78.2	Ref. [8]
CoS_2 NA/Ti	1.0 M KOH + 0.3 M urea	1.59	80.0	Ref. [9]
Ni@S-C-500	1.0 M KOH + 0.33 M urea	1.41	98.9	Ref. [10]
Ni@NCNT	1.0 M KOH + 0.5 M urea	1.38	76.1	Ref. [11]
a-Ni_2P/G	1.0 M KOH + 0.33 M urea	1.28	–	Ref. [12]
NiF_3/Ni_2P@CC-2	1.0 M KOH + 0.33 M urea	1.36	33	Ref. [13]
$Ni_2Fe(CN)_6$	1.0 M KOH + 0.33 M urea	1.34	–	Ref. [14]
$Ni_2P/N\text{-}C_{nanorods}$-2h	1.0 M KOH + 0.33 M urea	1.39	36.7	Ref. [15]
NiFe-PBA/NF	1.0 M KOH + 0.33 M urea	1.35	–	Ref. [16]
$NiWO_4\text{-}TA_{950}$	1.0 M KOH + 0.5 M urea	1.35	26.4	Ref. [17]
$Ni(OH)_2$/CuO NWs/CF	1.0 M KOH + 0.5 M urea	1.31	14	Ref. [18]
Rh-NCs/NiO-NSs	1.0 M KOH + 0.33 M urea	1.39	36.6	Ref. [19]
NCVS-3	1.0 M KOH + 0.33 M urea	1.36	–	Ref. [20]

Table S2. ICP-MS Investigations of the Electrolyte for PA-NF after UOR

Total electrolyte volume (mL)	Electrolyte volume for ICP-MS (mL)	Measured metal content (ppm)	Mass of leached metal in electrolyte (mg)	Mass of PA-NF (mg)	Metal loss (%)
40	4	1.0	0.04	55.4	0.1

Table S3. The Fitted EIS Parameters for NF and PA-NF at Various Potentials

Electrode	E [V *vs.* RHE]	R_s [Ω]	n_1	R_1 [Ω]	CPE_1 [F s^{n-1}]	R_2 [Ω]	C_2 [mF]
PA-NF	1.2	3.2	0.85	25.1	0.0033	251.2	1.0
	1.25	3.3	0.83	26.2	0.0046	95.5	4.0
	1.3	3.1	0.83	27.3	0.0079	33.1	13.0
	1.35	3.5	0.82	28.4	0.0117	12.0	33.1
	1.4	3.4	0.82	29.9	0.027	6.1	100.4
	1.45	3.6	0.87	30.1	0.0409	3.0	129.9
	1.5	3.0	0.86	31.3	0.0502	1.1	140.6
	1.55	3.2	0.85	31.7	0.0601	–	–
NF	1.2	3.5	0.85	27.1	0.0030	1368.1	2.4
	1.25	3.6	0.86	29.2	0.0028	750.2	3.4
	1.3	3.2	0.88	30.3	0.0058	354.8	3.8
	1.35	3.4	0.86	31.4	0.0147	151.4	6.7
	1.4	3.3	0.91	32.9	0.0216	74.1	13.0
	1.45	3.2	0.83	33.1	0.0339	36.3	21.0
	1.5	3.8	0.81	33.9	0.0510	10.8	22.0
	1.55	3.5	0.82	34.7	0.0612	–	–

Table S4. Calculated ECSA Values of Various Electrodes for UOR

Catalytic electrodes	C_{dl} [mF]	[a]ECSA [cm^2]
PA-NF	41.2	1030.0
NF	5.9	147.5

[a] ECSA = C_{dl}/0.040 mF cm^{-2}

n REFERENCES

(1) Liu, H.; Liu, Z.; Wang, F.; Feng, L. Efficient catalysis of N doped NiS/NiS_2 heterogeneous structure. *Chem. Eng. J.* **2020**, 397, 125507.
(2) Liu, Q.; Xie, L.; Qu, F.; Liu, Z.; Du, G.; Asiri, A. M.; Sun, X. A porous Ni_3N nanosheet array as a high-performance non-noble-metal catalyst for urea-assisted electrochemical hydrogen production. *Inorg. Chem. Front.* **2017**, 4, 1120-1124.
(3) Wang, X.; Wang, J.; Sun, X.; Wei, S.; Cui, L.; Yang, W.; Liu, J. Hierarchical coral-like NiMoS nanohybrids as highly efficient bifunctional electrocatalysts for overall urea electrolysis. *Nano Res.* **2018**, 11, 988-996.
(4) Xu, B.; Yang, X.; Liu, X.; Song, W.; Sun, Y.; Liu, Q.; Yang, H.; Li, C. Lattice distortion in hybrid $NiTe_2$/$Ni(OH)_2$ nanosheets as efficient synergistic electrocatalyst for water and urea oxidation. *J. Power Sources* **2020**, 449, 227585.
(5) Du, X.; Zhang, X. Dual-functional Co_3O_4@$Co_2P_4O_{12}$ nanoneedles supported on nickel foams with enhanced electrochemical performance and excellent stability for overall urea splitting. *Int. J. Hydrogen Energy* **2019**, 44, 24705-24711.
(6) Xiao, C.; Li, S.; Zhang, X.; MacFarlane, D. R. MnO_2/$MnCo_2O_4$/Ni heterostructure with quadruple hierarchy: a bifunctional electrode architecture for overall urea oxidation. *J. Mater. Chem. A* **2017**, 5, 7825-7832.
(7) Wang, L.; Ren, L.; Wang, X.; Feng, X.; Zhou, J.; Wang, B. Multivariate MOF-templated pomegranate-like Ni/C as efficient bifunctional electrocatalyst for hydrogen evolution and urea oxidation. *ACS Appl. Mater. Inter.* **2018**, 10, 4750-4756.
(8) Zhang, X.; Liu, Y.; Xiong, Q.; Liu, G.; Zhao, C.; Wang, G.; Zhang, Y.; Zhang, H.; Zhao, H. Vapour-phase hydrothermal synthesis of Ni_2P nanocrystallines on carbon fiber cloth for high-efficiency H_2 production and simultaneous urea decomposition. *Electrochim. Acta* **2017**, 254, 44-49.
(9) Wei, S.; Wang, X.; Wang, J.; Sun, X.; Cui, L.; Yang, W.; Zheng, Y.; Liu, J. CoS_2 nanoneedle array on Ti mesh: a stable and efficient bifunctional electrocatalyst for urea-assisted electrolytic hydrogen production. *Electrochim. Acta* **2017**, 246, 776-782.
(10) Wu, N.; Zhang, X.; Guo, R.; Ma, M.; Zhang, Y.; Hu, T. Nickel nanocrystal/sulfur-doped carbon composites as efficient and stable electrocatalysts for urea oxidation reaction. *J. Alloy. Comp.* **2022**, 163916.
(11) Zhang, Q.; Kazim, F. M.; Ma, S.; Qu, K.; Li, M.; Wang, Y.; Hu, H.; Cai, W.; Yang, Z. Nitrogen dopants in nickel nanoparticles embedded carbon nanotubes promote overall urea oxidation. *Appl. Catal. B-Environ.* **2021**, 280, 119436.
(12) Tong, Y.; Chen, L.; Dyson, P. J.; Fei, Z. Boosting hydrogen production via urea electrolysis on an amorphous nickel phosphide/graphene hybrid structure. *J. Mater. Sci.* **2021**, 56, 17709-17720.
(13) Wang, K.; Huang, W.; Cao, Q.; Zhao, Y.; Sun, X.; Ding, R.; Lin, W.; Liu, E.; Gao, P. Engineering NiF_3/Ni_2P heterojunction as efficient electrocatalysts for urea oxidation and splitting. *Chem. Eng. J.* **2022**, 427, 130865.
(14) Geng, S.-K.; Zheng, Y.; Li, S.-Q.; Su, H.; Zhao, X.; Hu, J.; Shu, H.-B.; Jaroniec, M.; Chen, P.; Liu, Q.-H. Nickel ferrocyanide as a high-performance urea oxidation electrocatalyst. *Nat. Energy* **2021**, 6, 904-912.
(15) Zhang, X.; Ma, G.; Shui, L.; Zhou, G.; Wang, X. Urea electrooxidation-boosted hydrogen production on nitrogen-doped porous carbon nanorod-supported nickel phosphide nanoparticles. *J. Energy Chem.* **2022**, doi.org/10.1016/j.jechem.2022.04.045.
(16) Jia, X.; Kang, H.; Yang, X.; Li, Y.; Cui, K.; Wu, X.; Qin, W.; Wu, G. Amorphous Ni(III)-based sulfides as bifunctional water and urea oxidation anode electrocatalysts for hydrogen generation from urea-containing water. *Appl. Catal. B-Environ.* **2022**, 312, 121389.
(17) Lin, R.; Kang, L.; Zhao, T.; Feng, J.; Celorrio, V.; Zhang, G.; Cibin, G.; Kucernak, A.; Brett, D. J. L.; Corà, F.; Parkin, I. P.; He, G. Identification and manipulation of dynamic active site deficiency-induced competing reactions in electrocatalytic oxidation processes. *Energy Environ. Sci.* **2022**, DOI: 10.1039/D1EE03522C.
(18) Sun, H.; Liu, J.; Chen, G.; Kim, H.; Kim, S.; Hu, Z.; Chen, J.-M.; Haw, S.-C.; Ciucci, F.; Jung, W. Hierarchical structure of CuO nanowires decorated with $Ni(OH)_2$ supported on Cu foam for hydrogen production via urea electrocatalysis. *Small Methods* **2022**, 6, 2101017.
(19) Ma, G.; Xue, Q.; Zhu, J.; Zhang, X.; Wang, X.; Yao, H.; Zhou, G.; Chen, Y. Ultrafine Rh nanocrystals decorated ultrathin NiO nanosheets for urea electro-oxidation. *Appl. Catal. B-Environ.* **2020**, 265, 118567.
(20) Ji, Z.; Song, Y.; Zhao, S.; Li, Y.; Liu, J.; Hu, W. Pathway manipulation via Ni, Co, and V ternary synergism to realize high efficiency for urea electrocatalytic oxidation. *ACS Catal.* **2021**, 12, 569-579.